Wireless Readout of Passive *LC* Sensors

Reinhard Nopper, Remigius Niekrawietz, and Leonhard Reindl, *Member, IEEE*

***Abstract*—This paper reports simple yet precise equations for automated wireless measurement of the resonance frequency, *Q*-factor, and coupling coefficient of inductively coupled passive resonant *LC* circuits. This allows remote sensing of all physical and chemical quantities that can be measured with capacitance transducers. Formerly reported front-end circuit concepts for wireless sensor readout, i.e., phase dip measurement and the dip meter, are subsequently discussed. It is shown that, due to fundamental system limitations, the formerly reported circuit concepts are not applicable if the distance between the sensor and the readout electronic circuit becomes too small, resulting in large coupling coefficients. Therefore, we present an improved concept for an analog front-end circuit of the readout system that overcomes these limitations and hence allows wireless sensor readout under a wider range of operating distances.**

***Index Terms*—Capacitance transducers, inductive coupling, *LC* circuits, remote sensing, resonance detection, telemetry.**

I. Introduction

MANY industrial, automotive, and medical applications require sensing of physical or chemical quantities at locations where a wired connection between the sensor and its evaluation circuit cannot be established. Examples of these applications are sensors on moving or rotating parts such as tire pressure measurement systems [1], medical sensing inside the human body such as intraocular eye pressure measurement [2], [3], or sensing under harsh environmental conditions, such as corrosive media or high temperature [4]. In particular, in the latter case, no damageable wire connections and electronic circuitry are desired at the point of measurement. Therefore, a completely passive and wireless sensor element is required. Passive wireless sensors for a variety of quantities to be measured such as temperature [1], pressure [2]–[5], humidity [6], strain [7], and chemical sensors [8] have been proposed in former publications. All these concepts are based on *LC* resonant circuits where the quantity to be measured affects the capacitance, which, in turn, affects the sensor's resonance frequency. Change in the resonance frequency can be detected by another inductively coupled coil that is connected to the signal-conditioning electronics.

Most publications focus on the design of the sensor element itself, which is usually a capacitor whose electrodes are deflected by mechanical forces, or the dielectric's relative permittivity is dependent on the quantity to be measured. Less research effort has been made to develop a robust and accurate readout system for these kinds of wireless sensors. In this paper, techniques for wireless measurement of the resonance frequency, Q-factor, and coupling coefficient of an inductively coupled LC sensor based on the air-core transformer-based system model are derived. Formerly published readout concepts for measuring the sensor's resonance frequency are examined for their suitability for automatic resonance detection in a sensor system, and their fundamental limitations will be shown. Finally, an improved readout circuit avoiding these limitations will be presented to be suitable for automatic resonance detection under a wide range of operation conditions.

Manuscript received June 2, 2009; revised August 5, 2009; accepted August 18, 2009. Date of publication October 30, 2009; date of current version August 11, 2010. The Associate Editor coordinating the review process for this paper was Dr. Juha Kostamovaara.

R. Nopper and R. Niekrawietz are with the Microsystem Technologies Department, Corporate Sector Research and Advance Engineering, Robert Bosch GmbH, 70839 Gerlingen-Schillerhöhe, Germany (e-mail: reinhard.nopper@de.bosch.com; remigius.niekrawietz@de.bosch.com).

L. Reindl is with the Laboratory of Electrical Instrumentation, Institute for Microsystem Technology (IMTEK), Albert-Ludwigs-Universität, 79110 Freiburg, Germany.

Digital Object Identifier 10.1109/TIM.2009.2032966

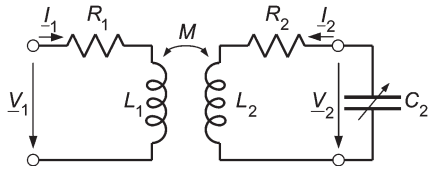

Fig. 1. Equivalent network of the inductively coupled sensor system.

II. System Model

A. Analytical Model

An analytical model of the inductively coupled sensor can be derived using the well-known transformer equations for harmonic oscillations with the frequency f using complex notation, i.e.,

$$\underline{V}_1 = R_1\underline{I}_1 + j2\pi f L_1\underline{I}_1 + j2\pi f M\underline{I}_2 \quad (1)$$

$$\underline{V}_2 = R_2\underline{I}_2 + j2\pi f L_2\underline{I}_2 + j2\pi f M\underline{I}_1 \quad (2)$$

where $\underline{V}_1$, $\underline{V}_2$, $\underline{I}_1$, and $\underline{I}_2$ are defined as shown in Fig. 1. The mutual inductance M of the coupled coils can be written as

$$M = k\sqrt{L_1 L_2} \quad (3)$$

where k is the geometry-dependent coupling coefficient with a value between 0 (no coupling) and ± 1 (maximum coupling). The sensor coil is terminated with the capacitance transducer C_2, i.e.,

$$\underline{I}_2 = -j2\pi f C_2\underline{V}_2. \quad (4)$$

The equivalent input impedance $\underline{Z}_1$ at the terminals of the readout coil is derived using (1), (2), and (4), i.e.,

$$\underline{Z}_1 = \frac{\underline{V}_1}{\underline{I}_1} = R_1 + j2\pi f L_1 + \frac{(2\pi f)^2 M^2}{R_2 + j\left(2\pi f L_2 - \frac{1}{2\pi f C_2}\right)}. \quad (5)$$

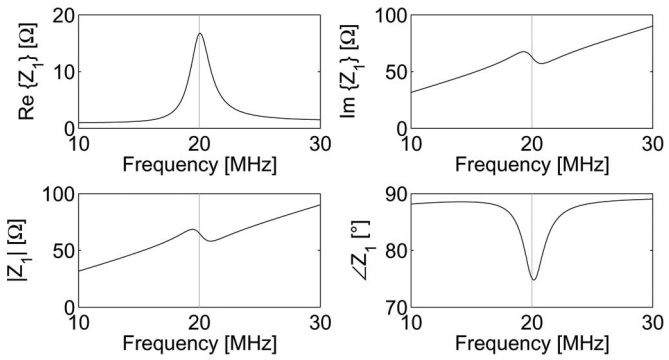

Fig. 2. Calculated impedance at the terminals of the readout coil with $R_1 = 1\ \Omega$, $L_1 = 0.5\ \mu$H, $f_2 = 20$ MHz (vertical line), $Q_2 = 10$, and $k = 0.05$.

Using the substitutions

$$f_2 = \frac{1}{2\pi\sqrt{L_2 C_2}} \tag{6}$$

$$Q_2 = \frac{1}{R_2}\sqrt{\frac{L_2}{C_2}} \tag{7}$$

where Q_2 is the Q-factor, and f_2 is the resonance frequency of the sensor circuit; $\underline{Z}_1$ can be rewritten (8) and split up into a real part (9) and an imaginary part (10), i.e.,

$$\underline{Z}_1 = R_1 + j2\pi f L_1 \left(1 + \frac{k^2\left(\frac{f}{f_2}\right)^2}{1 + j\frac{1}{Q_2}\frac{f}{f_2} - \left(\frac{f}{f_2}\right)^2}\right) \tag{8}$$

$$\mathrm{Re}\{\underline{Z}_1\} = R_1 + 2\pi f L_1 k^2 Q_2 \frac{\frac{f}{f_2}}{1 + Q_2^2\left(\frac{f}{f_2} - \frac{f_2}{f}\right)^2} \tag{9}$$

$$\mathrm{Im}\{\underline{Z}_1\} = 2\pi f L_1 \left(1 + k^2 Q_2^2 \frac{1 - \left(\frac{f}{f_2}\right)^2}{1 + Q_2^2\left(\frac{f}{f_2} - \frac{f_2}{f}\right)^2}\right). \tag{10}$$

With (9) and (10), the modulus $|\underline{Z}_1|$ and phase $\angle\underline{Z}_1$ of the input impedance is

$$|\underline{Z}_1| = \sqrt{\mathrm{Re}^2\{\underline{Z}_1\} + \mathrm{Im}^2\{\underline{Z}_1\}} \tag{11}$$

$$\angle\underline{Z}_1 = \arctan\frac{\mathrm{Im}\{\underline{Z}_1\}}{\mathrm{Re}\{\underline{Z}_1\}}. \tag{12}$$

Equations (8)–(10) show that only two independent parameters of the sensor circuit, i.e., the Q-factor and the resonance frequency, can be obtained by wireless measurement. The calculated frequency response of the impedance at the terminals of the readout coil is shown in Fig. 2 using assumed system parameters.

B. Experimental Results

The analytical model presented was verified by impedance measurement of inductively coupled *LC* resonance circuits. First, simple expressions have been derived from the analytical model to calculate the system parameters k, Q_2, and f_2 from measured data. Subsequently, the experimentally determined parameters were used to fit the analytical model to the measured impedance plots. This approach provides a fair estimation of whether the analytical model is appropriate to describe the behavior of a real inductively coupled sensor system. The inductance L_1 and the ohmic series resistance R_1 of the readout coil can be read off the measured frequency response of $\underline{Z}_1$ for low frequencies (i.e., $f \approx 0$) or if the sensor is removed (i.e., $k = 0$), i.e.,

$$L_1 = \frac{1}{2\pi}\left.\frac{\partial \mathrm{Im}\{\underline{Z}_1\}}{\partial f}\right|_{(f\approx 0)\vee(k=0)} \tag{13}$$

$$R_1 = \mathrm{Re}\{\underline{Z}_1\}|_{(f\approx 0)\vee(k=0)}. \tag{14}$$

The resonance frequency f_2 can be obtained from the maximum of $\mathrm{Re}\{\underline{Z}_1\}$ with respect to f, i.e.,

$$f_{\max} = \frac{2Q_2}{\sqrt{4Q_2^2 - 2}} f_2. \tag{15}$$

If Q_2 is large, compared to unity, (15) can be simplified as

$$f_{\max} \approx f_2. \tag{16}$$

The Q-factor-dependent prefactor in (15) is the relative error that will be made if $f_{\max}$ is assumed to be the sensor resonance frequency. The relative error is 1% if $Q_2 = 5$ and 0.1% if $Q_2 = 16$. With low Q_2 values or if a high accuracy in measuring f_2 is required, the Q-factor-dependent correction factor must be taken into account according to (15). For this purpose, Q_2 is determined as described here.

The maximum value of $\mathrm{Re}\{\underline{Z}_1\}$ at $f = f_{\max}$ is $Z_{\mathrm{r1,max}}$, as shown in the following:

$$Z_{\mathrm{r1,max}} = \mathrm{Re}\{\underline{Z}_1\}|_{f=f_{\max}} = R_1 + \frac{8\pi f_2 L_1 k^2 Q_2^3}{4Q_2^2 - 1} \tag{17}$$

$$\approx R_1 + 2\pi f_2 L_1 k^2 Q_2 \tag{18}$$

which can be simplified to (18), if Q_2 is large, compared to unity. To obtain Q_2, the limiting frequencies of the full width at half maximum (FWHM) bandwidth $f_{\mathrm{FWHM1,2}}$ are calculated, where

$$\frac{\mathrm{Re}\{\underline{Z}_1\}|_{f=f_{\mathrm{FWHM1,2}}} - R_1}{Z_{\mathrm{r1},max} - R_1} = \frac{1}{2}. \tag{19}$$

The absolute difference between f_{FWHM1} and f_{FWHM2} is the FWHM bandwidth Δf_{FWHM}, which is given by

$$\Delta f_{\mathrm{FWHM}} = |f_{\mathrm{FWHM2}} - f_{\mathrm{FWHM1}}|. \tag{20}$$

Assuming that Q_2 is large, compared to unity, Q_2 can be calculated by solving (19) for Δf_{FWHM} using (9) and (17) as

$$Q_2 \approx \frac{f_2}{\Delta f_{\mathrm{FWHM}}}. \tag{21}$$

The actual value of Q_2 is slightly larger than the approximated value according to (21). Fig. 3 shows the relative error $\Delta Q_2/Q_2$ made when using (21). If Q_2, f_2, L_1, and R_1 are known, k can be calculated from (18) as

$$k \approx \sqrt{\frac{Z_{\mathrm{r1,max}} - R_1}{2\pi f_2 L_1 Q_2}}. \tag{22}$$

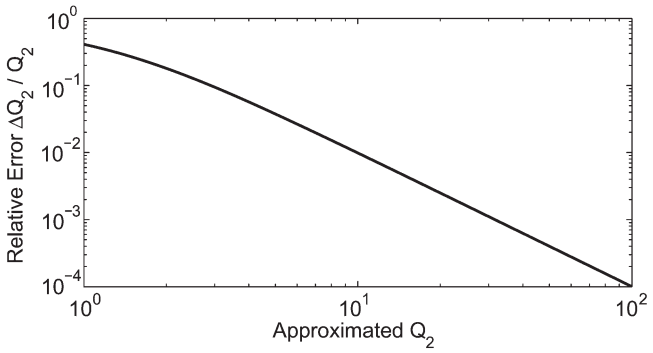

Fig. 3. Relative error made when using (21) for approximating Q_2.

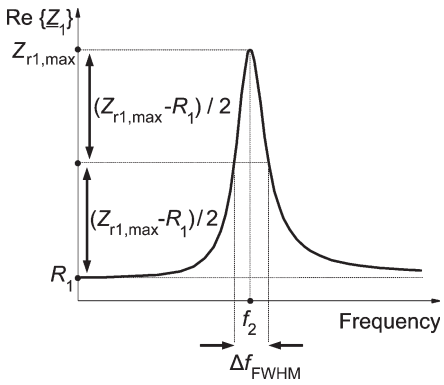

Fig. 4. $\mathrm{Re}\{\underline{Z}_1\}$ with parameters for calculating the analytical curve fit.

TABLE I
DESIGN PARAMETERS OF THE MEASURED PCB COILS

	Readout coil	Sensor coil
Conductor width	70 μm	70 μm
Conductor height	18 μm	18 μm
Spacing	70 μm	70 μm
No. of turns	8	8
Diameter	15 mm	12 mm

Fig. 4 summarizes the needed parameters for fitting the analytical equations (8)–(10) for the readout coil impedance to a measured $\underline{Z}_1$ curve.

Measurements have been performed with planar spiral copper coils fabricated on printed circuit boards (PCBs). The sensor circuit was emulated by a capacitance trimmer at the terminals of the sensor coil. The readout coil circuit board was provided with an SMB connector to plug an HP 8753D vector network analyzer used for frequency-dependent impedance measurement. The IF bandwidth of the network analyzer was set to 3 kHz. Proper coaxial alignment of the sensor coil to the readout coil was assured by using vertical pins plugged into pinholes on both circuit boards. The vertical distance between the coils was adjusted with ceramic spacers. Table I summarizes the design parameters of the used PCB coils. The test setup used is shown in Fig. 5. The dashed black line in Fig. 6 shows a measured impedance plot taken at a distance of 2.95 mm between the coaxially aligned sensor and readout coils. From this plot, R_1, L_1, f_2, Q_2, and k were determined by Matlab using the formulas previously derived. Table II summarizes the obtained system parameters, along with the standard deviation of the measured and calculated values. For calculating the standard deviation, the statistical error of the impedance measurement has been estimated and was propagated to the other parameters derived. The measured values were used to fit the analytical model according to (8)–(10). The result is plotted as a continuous gray line in Fig. 6. The influence of the sensor to $\mathrm{Im}\{\underline{Z}_1\}$ in Fig. 6 is fairly strong, compared to the calculated plot in Fig. 2 due to the high k value of 0.25 and the quadratic dependence of the right term in (10) of k. The measured frequency response of the impedance is shown to match very well with the predicted shape. However, for higher frequencies, the parasitic interwinding capacitance of the readout coil must also be taken into account. As a first approximation, the interwinding capacitance is modeled as a capacitor C_{L_1} in parallel with L_1 and R_1. This results in the self-resonance frequency of the readout coil as

$$f_{L_1} \approx \frac{1}{2\pi\sqrt{L_1 C_{L_1}}}. \tag{23}$$

A network analyzer measurement showed that the parallel self-resonance of the used readout coil is approximately at 150 MHz, implying that $C_{L_1} = 1/(4\pi^2 f_{L_1}^2 L_1) \approx 0.6$ pF. Since, at 20 MHz, the absolute reactance of C_{L_1} is more than 50 times higher than the reactance of L_1, the value of C_{L_1} is small enough to be neglected. However, in general, the readout coil must appropriately be designed, so that its self-resonance does not interfere with the sensor resonance. This can be done by carefully choosing the number of turns, coil diameter, conductor height, and spacing between the windings. Using the values shown in Table II, the coupling coefficient has been calculated for different distances between the coaxially aligned coils from 0.2 to 14.7 mm. The resulting k values are shown in Fig. 7. To check that the k measurements are reasonable, the coupling coefficient has been calculated with Matlab, as reported in [9]. For the analytical calculation according to [9], two major approximations were made: the coils were assumed to be made up of concentric circular conductor loops, instead of a spiral, and the radius of each conductor loop was assumed to be large, compared to the width of the conducting wire. In addition to the analytical k calculation, the coupled coils have been simulated using the commercial simulation tool CST Microwave Studio (CST MWS). CST MWS is based on the finite integration technique, which is a very general approach that describes Maxwell's equations on a grid space, can be written in time and frequency domains, and is not restricted to a specific grid type.

The results of the calculation and the simulation using the geometrical parameters of the used planar coils are also shown in Fig. 7. Both of these curves are in very good agreement with the measurement results showing a relative deviation from the measured values of less than 10%. According to Table II, the relative standard deviation of the k measurement is estimated to be about 6%, which was calculated at a distance of 2.95 mm. The remaining systematic error can be explained with the approximations made for the analytical calculation and small geometry differences between the real test setup and the simulated and calculated ideal setups due to fabrication tolerances. Another important difference is the presence of metallic objects near the coil such as the SMB connector and

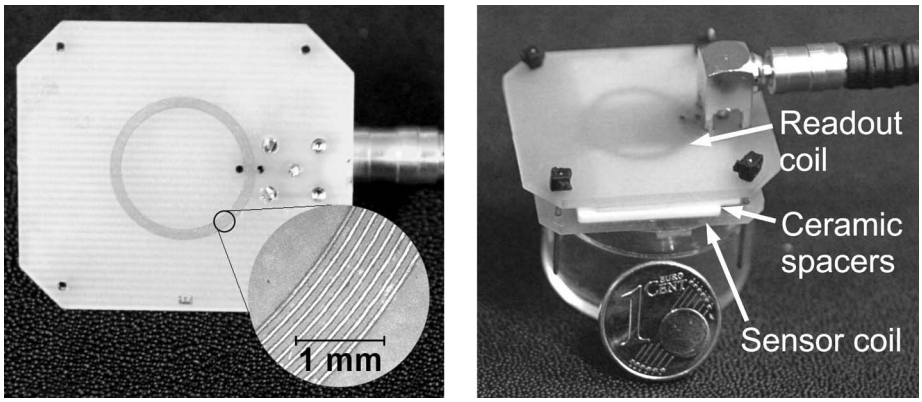

Fig. 5. (Left) Readout coil on PCB. (Right) Complete test setup.

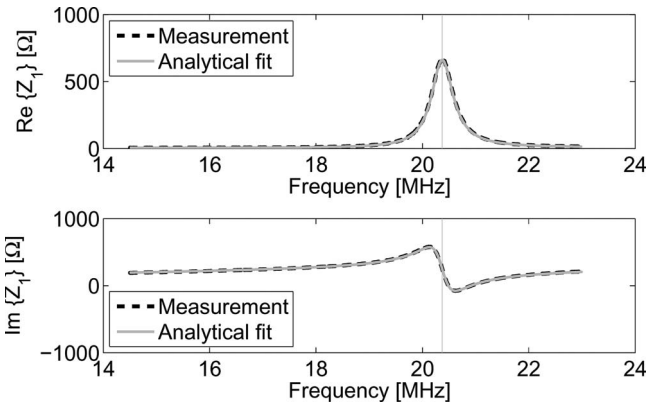

Fig. 6. Measured impedance, compared to the fitted analytical model. The vertical line marks the sensor resonance frequency at 20.37 MHz.

TABLE II
SYSTEM PARAMETERS OBTAINED FROM IMPEDANCE MEASUREMENT AT 2.95-mm DISTANCE

	L_1	R_1	f_2	Q_2	k
Mean	2 μH	5.5 Ω	20.37 MHz	41	0.25
Std. dev.	60 nH	0.3 Ω	30 kHz	0.2	0.015
	$\widehat{=}$ 3%	$\widehat{=}$ 5.5%	$\widehat{=}$ 0.15%	$\widehat{=}$ 0.49%	$\widehat{=}$ 6%

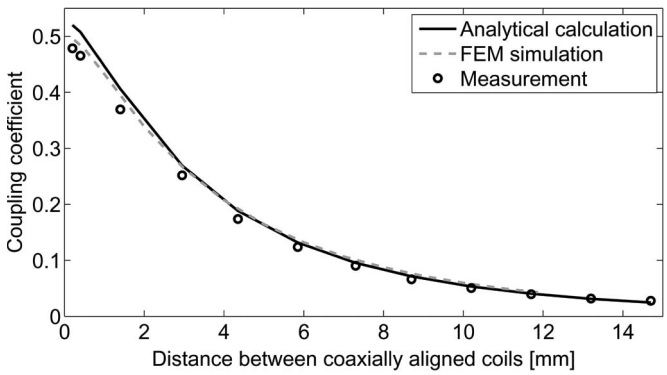

Fig. 7. Coupling coefficient k versus distance for the used planar PCB coils.

the electrical connection of the coils. Eddy currents induced within these conducting areas cause a weakened magnetic field, compared to the ideal setup, and therefore a slightly lower coupling coefficient k. The systematical error caused by the approximated equations (18) and (22) is negligible for $Q_2 = 41$, compared to the other error sources.

III. READOUT CIRCUIT ARCHITECTURES

In this section, formerly reported concepts for wireless readout of *LC* sensors are examined for their suitability for automatically measuring the sensor resonance frequency in a wireless sensing system. The readout system must be simple enough to be implemented in a low-cost application-specific integrated circuit for large-scale production. Automated resonance detection should be possible under a wide range of coupling conditions.

All architectures discussed are based on frequency-dependent measurement of the impedance of the readout coil. Other readout concepts such as harmonics detection [10] did not seem promising since additional components such as diodes are required in the sensor. This would increase production costs without offering conclusive advantages [11].

A. Phase Dip Measurement

Measuring the characteristic impedance phase dip, as shown in Fig. 2, to determine the sensor resonance frequency has been proposed in several publications, e.g., [5], [8], and [12]. The impedance phase $\angle \underline{Z}_1$, as given in (12), can be measured using an impedance or network analyzer. However, the position of the phase minimum is not independent of the coupling coefficient, as shown in Fig. 8. For increasing k values, the phase dip becomes broader, with the phase minimum being shifted to higher frequencies. Assuming $Q_2 \gg 1$ and neglecting R_1, the frequency of the impedance phase minimum is

$$f_{\varphi,\min} = \sqrt{\frac{k^2 - 2 + \sqrt{k^4 - 16k^2 + 16}}{2 - 2k^2}}\, f_2. \tag{24}$$

Taylor series expansion of (24) close to $k = 0$ results in the quadratic approximation

$$f_{\varphi,\min} \approx \left(1 + \frac{1}{4}k^2\right) f_2. \tag{25}$$

Assuming that the relative deviation of $f_{\varphi,\min}$ from f_2 should be lower than 0.1%, then according to (25), k must be lower than 0.06. With the used coils, this corresponds to a distance of approximately 10 mm. At this distance, the phase dip is only about 8° deep with the used coils. In general, a small phase dip

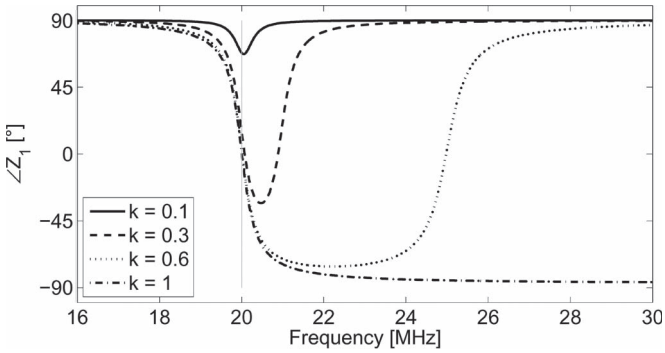

Fig. 8. Calculated impedance phase at different k values with $f_2 = 20$ MHz (vertical line), $Q_2 = 40$, and $L_1 = 2\ \mu$H.

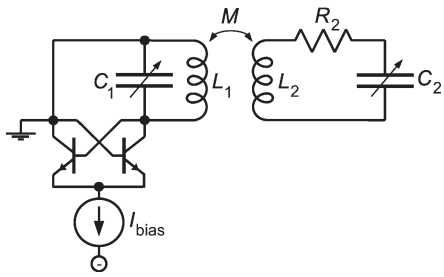

Fig. 9. Example basic dip meter circuit based on a cross-coupled oscillator.

results in a poor signal-to-noise ratio. Phase dip measurement is therefore only reasonable for a relatively small range of k values, where the distance of the sensor is small enough to generate a sufficiently strong signal but large enough to avoid signal distortion.

B. Dip Meter Measurement

Measuring the real part, instead of the phase, of the read out coil impedance is more advantageous since (15) shows that the frequency of maximal $\mathrm{Re}\{\underline{Z}_1\}$ is independent of k. The frequency-dependent portion of $\mathrm{Re}\{\underline{Z}_1\}$ can be interpreted as an additional resistance in the readout coil caused by inductive power transfer to the sensor circuit. Thus, the sensor decreases the effective Q-factor of the readout coil near the sensor resonance frequency

$$Q_{L_1,\mathrm{eff}} = \frac{2\pi f L_1}{\mathrm{Re}\{\underline{Z}_1\}}. \tag{26}$$

A circuit architecture for wireless measurement of resonance frequencies that utilizes the aforementioned effect is the dip meter. This technique has been proposed for wireless *LC* sensor readout in [3] and [7]. A dip meter is an *LC* oscillator, where the inductance of the *LC* tank is the readout coil inductively coupled to the resonant circuit to be measured. An example basic circuit implementation of a dip meter is shown in Fig. 9, where a cross-coupled differential pair oscillator architecture is used. The readout circuit will start oscillating with the frequency

$$f_1 = \frac{1}{2\pi\sqrt{L_1 C_1}}. \tag{27}$$

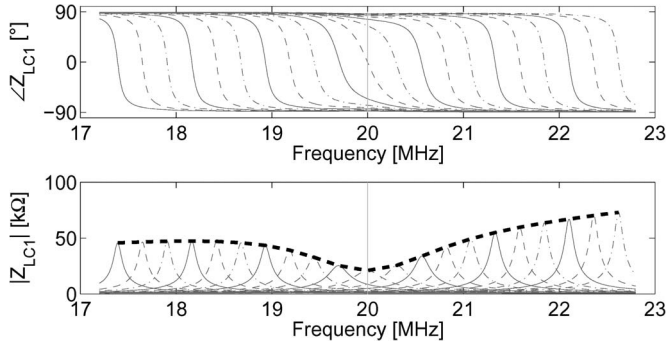

Fig. 10. Calculated impedance dip $f_2 = 20$ MHz (vertical line), $Q_2 = 20$, $L_1 = 2\ \mu$H, $R_1 = 1\ \Omega$, $k = 0.02$, and 24 pF $\leq C_1 \leq$ 40 pF.

The effective Q-factor of the readout *LC* resonator $Q_{1,\mathrm{eff}}$, taking the additional load caused by the nearby sensor into account, is

$$Q_{1,\mathrm{eff}} = \frac{1}{\mathrm{Re}\{\underline{Z}_1\}|_{f=f_1}}\sqrt{\frac{L_1}{C_1}}. \tag{28}$$

The total impedance of the readout tank

$$\underline{Z}_{\mathrm{LC1}} = \underline{Z}_1 \left\| \left(\frac{1}{j2\pi f C_1}\right) \right. \tag{29}$$

is shown in Fig. 10 for different C_1 values. The resonance resistance R_{LC1} of the readout tank is defined as the (real-valued) impedance at f_1

$$R_{\mathrm{LC1}} = \underline{Z}_{\mathrm{LC1}}|_{f=f_1} \tag{30}$$

$$= Q_{1,\mathrm{eff}}\sqrt{\frac{L_1}{C_1}} \tag{31}$$

$$= \frac{1}{\mathrm{Re}\{\underline{Z}_1\}|_{f=f_1}}\frac{L_1}{C_1}. \tag{32}$$

In Fig. 10, the decrease in R_{LC1} and, thus, $Q_{1,\mathrm{eff}}$ around the sensor resonance frequency, due to an increase in $\mathrm{Re}\{\underline{Z}_1\}$, is displayed. A lower effective Q-factor of the resonator requires a higher amplification of the differential pair to sustain a stable oscillation. In the given oscillator circuit, amplification is set by the bias current I_{bias}. A control loop readjusting I_{bias} can be incorporated, so that the oscillation voltage amplitude at the *LC* tank remains constant. Then, the required bias current can be used as a quantity for detecting sensor resonance.

However, according to (8)–(10), the sensor affects not only the Q-factor but also the reactance of the readout coil. This disturbs the oscillation behavior of the readout circuit. The modulus and phase of $\underline{Z}_{\mathrm{LC1}}$ for different k values are shown in Fig. 11. For small k values, the phase of $\underline{Z}_{\mathrm{LC1}}$ has a unique zero for all C_1 values at the frequency f_1. In this case, the circuit will start oscillating at f_1 and can be operated as previously described. If k has a critical value $k_{\max}$, the zero of the phase is a saddle point, when the readout oscillator's resonance frequency f_1 is close to the sensor resonance frequency f_2. At higher k values and for $f_1 \approx f_2$, three zeroes of the phase occur, corresponding to one serial and two parallel resonance frequencies. In practice, this effect has been observed as a frequency jump from the lower to the higher parallel resonance

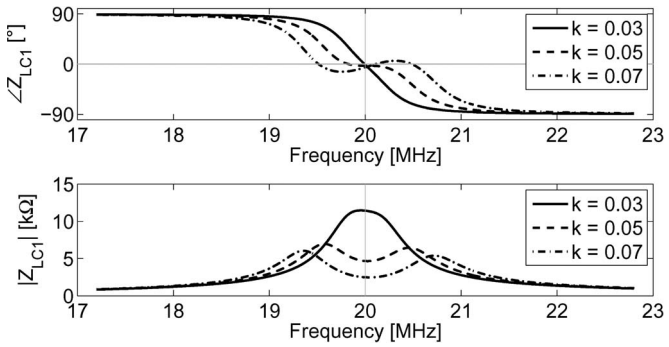

Fig. 11. Frequency response of $\underline{Z}_{\mathrm{LC1}}$ for different k values with $f_1 = f_2 = 20$ MHz (vertical line), $Q_2 = 20$, $L_1 = 2\ \mu$H, and $R_1 = 1\ \Omega$.

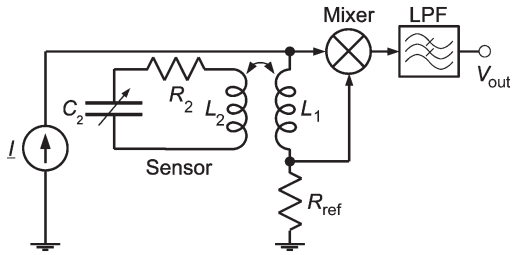

Fig. 12. Proposed front-end circuit for measuring $\mathrm{Re}\{\underline{Z}_1\}$.

frequency, when C_1 is slowly decreased and the sensor is close to the readout coil. The critical coupling coefficient $k_{\max}$ has been calculated by solving

$$\left.\frac{\partial \angle \underline{Z}_{\mathrm{LC1}}}{\partial f}\right|_{f=f_1=f_2} = 0 \tag{33}$$

for k. For simplification, the approximations $Q_2 \gg 1$ and $k \ll 1$ had to be assumed. The thereby obtained result is

$$k_{\max} \approx \frac{1}{Q_2} \tag{34}$$

which retrospectively validates the assumption $k \ll 1$. The actual coupling coefficient k should considerably be below $k_{\max}$, because a too flat slope of the phase of $\underline{Z}_{\mathrm{LC1}}$ around the zero would result in poor frequency noise behavior of the dip meter oscillator. Fig. 11 also shows that the amplitude of $\underline{Z}_{\mathrm{LC1}}$ at $f = f_1 = f_2$ starts to decrease with increasing k values and becomes a local minimum, even before $k = k_{\max}$. This effect will further decrease the tendency to start oscillation at f_1, if the value of k is too close at $k_{\max}$. In the test setup based on PCB coils, $k_{\max}$ is as low as 0.025 due to a sensor Q-factor of about 40. This $k_{\max}$ value corresponds to a minimum distance between the sensor and the readout coil of about 15 mm.

C. Proposed Impedance Measurement System

To overcome the limitations of the known dip meter circuit concerning distance, a novel readout front end for measuring $\mathrm{Re}\{\underline{Z}_1\}$ is proposed. Its basic architecture is shown in Fig. 12. The readout coil L_1 is driven by a variable-frequency ac current $\underline{I}$. Coherent demodulation of the voltage across the coil using a reference voltage $\underline{V}_{\mathrm{ref}}$ that is in phase with $\underline{I}$ is performed. $\underline{V}_{\mathrm{ref}}$ is generated using the ohmic resistance R_{ref} in series with L_1. The in-phase demodulation of the voltage signal cancels out the 90° phase-shifted voltage caused by the coil reactance and leaves a signal proportional to the real part of the current source's load impedance. Connecting R_{ref} in series with the readout coil ensures a proper phase relation between the voltages to be multiplied. Multiplication of the voltages by using a Gilbert cell mixer [13] and then low-pass filtering the output of the mixer results in the output dc voltage V_{out}, which is related to $\mathrm{Re}\{\underline{Z}_1\}$ as follows:

$$V_{\mathrm{out}} \propto R_{\mathrm{ref}} \cdot (R_1 + R_{\mathrm{ref}} + \mathrm{Re}\{\underline{Z}_1\}) \tag{35}$$

where the $R_1 + R_{\mathrm{ref}}$ term in the brackets causes a constant offset of V_{out} additional to the desired $\mathrm{Re}\{\underline{Z}_1\}$ proportionality. A system simulation of the proposed reader circuit has been performed using LTspice IV with the measured system parameters, as shown in Table II. The unknown value of L_2 was assumed to be 1.5 μH. Low-pass filtering was simulated by averaging the output of the mixer over the whole simulation period. Fig. 13 shows the simulated system and the obtained output voltage. The output voltage frequency response in Fig. 13 well shows the maximum indicating sensor resonance. The constant voltage offset of the resonance curve is caused by the additive R_{ref} term in (35) and the parasitic 5.5 Ω series resistance of the coil.

The proposed architecture for an analog front-end circuit has no fundamental limitations concerning the coupling coefficient. It is therefore also applicable if the distance between the coils becomes too low for proper operation of the previously presented architectures. If the distance between the coils is too small, then the capacitance between the coils will not be negligible though. A SPICE simulation showed that an additional capacitance between the coils causes a small shift of the measured resonance frequency to lower values. However, in our test setup, no such effect has been observed for distances longer than 0.5 mm. If very small distances are required, then the capacitance between the coils can be decreased by a suitable coil design. For example, choosing different coil diameters will minimize the overlapping area of the windings and therefore decrease capacitive coupling. Following the analog front-end circuit, a digital signal processing and control system for detecting the resonance frequency and controlling the ac current source frequency has to be implemented. In applications where measuring the sensor Q-factor is required, it can be determined by measuring either the FWHM cutoff frequencies as previously described or the curvature of $\mathrm{Re}\{\underline{Z}_1\}$ around its maximum. In the latter case, it is necessary to also measure k since, according to (9), the curvature of $\mathrm{Re}\{\underline{Z}_1\}$ is proportional to k^2. In general, at least three frequencies around the resonance frequency have to be sampled to determine f_2, Q_2, and k.

IV. Conclusion and Outlook

The Q-factor, resonance frequency, and coupling coefficient of an inductively coupled capacitance transducer can be determined from the frequency response of the readout coil impedance $\underline{Z}_1$. For this purpose, simple yet precise equations have been derived and exemplified.

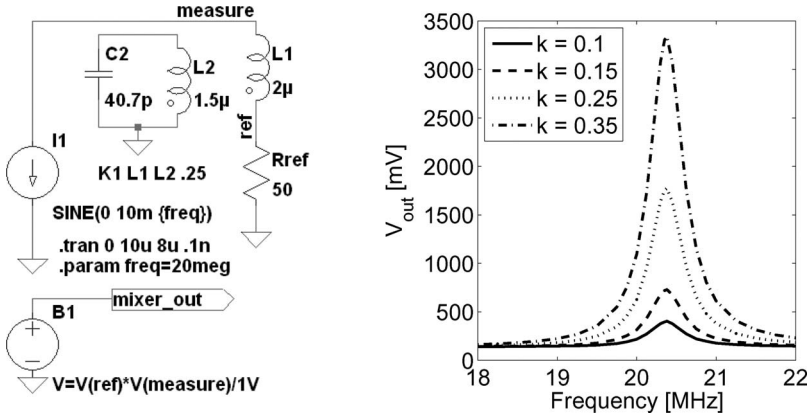

Fig. 13. SPICE simulation of V_{out}; $L_2 = 1.5\ \mu$H, $C_2 = 40.7$ pF, $R_2 = 4.68\ \Omega$, $L_1 = 2\ \mu$H, $R_1 = 5.5\ \Omega$, $R_{\text{ref}} = 50\ \Omega$, and $|\underline{I}| = 10$ mA.

Several methods for wireless readout of passive *LC* sensors have been discussed. Phase dip measurement shows a strong dependence on the coupling coefficient, particularly for high values of the coupling coefficient, i.e., low distances between the coils. It was shown that the real part of the readout coil impedance is a more appropriate quantity to determine the resonance frequency and Q-factor of the sensor, because its fundamental shape is coupling independent. The dip meter as a common circuit for measuring the real part of the readout coil impedance has been studied. It was derived that, due to the influence of the sensor to the readout coil reactance, a maximal allowed coupling coefficient that is approximately the reciprocal Q-factor of the sensor exists. The basic architecture of a novel analog front-end circuit for measuring the real part of the readout coil impedance that avoids this fundamental limitation of the dip meter has been presented.

Future work will focus on implementing a hardware demonstrator for the wireless readout system based on the analog front-end concept introduced in this paper. A digital signal processing unit following the analog front-end circuit has to be designed to detect the resonance peak and control the excitation frequency for the readout coil. Additional measurement of the sensor Q-factor is also possible. This might enable the compensation of the unwanted temperature cross-sensitivity.

REFERENCES

[1] M. Nabipoor and B. Y. Majlis, "A new passive telemetry LC pressure and temperature sensor optimized for TPMS," *J. Phys., Conf. Ser.*, vol. 34, pp. 770–775, Apr. 2006.
[2] C. C. Collins, "Miniature passive pressure transensor for implanting in the eye," *IEEE Trans. Biomed. Eng.*, vol. BME-14, no. 2, pp. 74–83, Apr. 1967.
[3] J. Coosemans, M. Catrysse, and R. Puers, "A readout circuit for an intra-ocular pressure sensor," *Sens. Actuators A, Phys.*, vol. 110, no. 1–3, pp. 432–438, Feb. 2004.
[4] M. A. Fonseca, J. M. English, M. von Arx, and M. G. Allen, "Wireless micromachined ceramic pressure sensor for high-temperature applications," *J. Microelectromech. Syst.*, vol. 11, no. 4, pp. 337–343, Aug. 2002.
[5] A. Baldi, W. Choi, and B. Ziaie, "A self-resonant frequency-modulated micromachined passive pressure transensor," *IEEE Sensors J.*, vol. 3, no. 6, pp. 728–733, Dec. 2003.
[6] K. G. Ong and C. A. Grimes, "A resonant printed-circuit sensor for remote query monitoring of environmental parameters," *Smart Mater. Struct.*, vol. 9, no. 4, pp. 421–428, Aug. 2000.
[7] J. C. Butler, A. J. Vigliotti, F. W. Verdi, and S. M. Walsh, "Wireless, passive, resonant-circuit, inductively coupled, inductive strain sensor," *Sens. Actuators A, Phys.*, vol. 102, no. 1/2, pp. 61–66, Dec. 2002.
[8] J. Garcia-Canton, A. Merlos, and A. Baldi, "High-quality factor electrolyte insulator silicon capacitor for wireless chemical sensing," *IEEE Electron Device Lett.*, vol. 28, no. 1, pp. 27–29, Jan. 2007.
[9] C. M. Zierhofer and E. S. Hochmair, "Geometric approach for coupling enhancement of magnetically coupled coils," *IEEE Trans. Biomed. Eng.*, vol. 43, no. 7, pp. 708–714, Jul. 1996.
[10] K. Van Schuylenbergh and R. Puers, "Passive telemetry by harmonics detection," in *Proc. IEEE EMBC*, 1996, pp. 299–300.
[11] J. Coosemans, M. Catrysse, T. Aerts, and R. Puers, "A read-out circuit for an intra-ocular pressure sensor," in *Proc. Eurosensors XVI*, 2002, pp. 533–536.
[12] T. J. Harpster, S. Hauvespre, M. R. Dokmeci, and K. Najafi, "A passive humidity monitoring system for in situ remote wireless testing of micropackages," *J. Microelectromech. Syst.*, vol. 11, no. 1, pp. 61–67, Feb. 2002.
[13] B. Gilbert, "A precise four-quadrant multiplier with subnanosecond response," *IEEE J. Solid-State Circuits*, vol. SSC-3, no. 4, pp. 365–373, Dec. 1968.

Reinhard Nopper was born in Berlin, Germany, in 1982. He received the Dipl.-Ing. degree in electrical engineering from Ulm University, Ulm, Germany, in 2007. He is currently working toward the Ph.D. degree with the Microsystem Technologies Department, Corporate Sector Research and Advance Engineering, Robert Bosch GmbH, Gerlingen, Germany.

His research interests include concepts for wireless microelectromechanic sensors and sensor readout circuitry.

Remigius Niekrawietz received the Dipl.-Ing. degree in microsystem technology from Albert-Ludwigs-Universität, Freiburg, Germany, in 2003. He is currently working toward the Ph.D. degree with Albert-Ludwigs-Universität.

From 2003 to 2006, he was a Research Assistant with the Laboratory for MEMS Applications, Institute for Microsystem Technology (IMTEK), Albert-Ludwigs-Universität. He pioneered the development of TopSpot printing technology for high-throughput microarray fabrication. He is currently with the Microsystem Technologies Department, Corporate Sector Research and Advance Engineering, Robert Bosch GmbH, Gerlingen, Germany, where he works in the field of modeling and simulation for the design of microelectromechanical systems.

Leonhard Reindl (M'93) received the Dipl. Phys. degree from the Technical University of Munich, Munich, Germany, in 1985 and the Dr. Sc. Techn. degree from the University of Technology Vienna, Vienna, Austria, in 1997.

From 1985 to 1999, he was a member of the Microacoustics Group of the Siemens Corporate Technology Department, Munich, where he was engaged in research and development on surface acoustic wave (SAW) convolvers, dispersive and tapped delay lines, ID tags, and wireless passive SAW sensors. From 1999 to 2003, he was a University Lecturer of communication and microwave techniques with the Institute of Electrical Information Technology, Clausthal University of Technology, Clausthal-Zellerfeld, Germany. In May 2003, he joined the Laboratory for Electrical Instrumentation, Institute for Microsystem Technology (IMTEK), Albert-Ludwigs-Universität, Freiburg, Germany, as a Full Professor. He is the holder of 35 patents on SAW devices and wireless passive sensor systems. He has authored or coauthored approximately 130 papers. His research interests include wireless sensor and identification systems, SAW devices and materials, and microwave communication systems based on SAW devices.

Mr. Reindl is a member of the Technical Program Committee of the IEEE Frequency Control Symposium. He is also engaged in technical committees of the German VDE/ITG Association.